Chinese Chemical Letters 33 (2022) 2605–2610

Contents lists available at ScienceDirect

Chinese Chemical Letters

journal homepage: www.elsevier.com/locate/cclet

Self-assembly of three Ag-polyoxovanadates frameworks for their efficient construction of C–N bond and detoxification of simulant sulfur mustard

Xianqiang Huang[a,*], Yanan Cui[a], Jinhong Zhou[a], Yalin Zhang[a], Guodong Shen[a], Qingxia Yao[a], Jikun Li[b,*], Zechun Xue[a], Guoping Yang[c,*]

[a] Shandong Provincial Key Laboratory of Chemical Energy Storage and Novel Cell Technology, School of Chemistry & Chemical Engineering, Liaocheng University, Liaocheng 252059, China
[b] College of Chemistry and Chemical Engineering, Taishan University, Taian 271021, China
[c] Jiangxi Province Key Laboratory of Synthetic Chemistry, Jiangxi Key Laboratory for Mass Spectrometry and Instrumentation, East China University of Technology, Nanchang 330013, China

ARTICLE INFO

Article history:
Received 18 August 2021
Revised 2 September 2021
Accepted 10 September 2021
Available online 16 September 2021

Keywords:
Ag-polyoxovanadates
Crystal engineering
Controllable synthesis
Bifunctional catalysts
Heterogeneous reaction

ABSTRACT

Three imidazole-modified Ag-polyoxovanadates frameworks (APFs) with a controllable molar ratio of Ag^+ to polyoxovanadates (POVs) $[Ag(IM)_2]_2V_4O_{12}\cdot 2Ag(IM)_2$ (**APF-1**), $[Ag_2(1\text{-eIM})_4]_2[Ag(1\text{-eIM})_2]_3\cdot 2Ag(1\text{-eIM})_2\cdot 3(1\text{-HeIM})[V_{10}O_{28}]_2$ (**APF-2**) and $[Ag(1\text{-pIM})_2]_3[HV_{10}O_{28}]\cdot 2Ag(1\text{-pIM})_2\cdot 2H_2O$ (**APF-3**) (IM = imidazole; 1-eIM = 1-ethylimidazole and 1-pIM = 1-propylimidazole) have been successfully achieved by self-assembly of POVs, Ag^+ cations, and three different imidazole derivatives. Interestingly, the molar ratios of Ag^+ to POVs vary from 4:1, 4.5:1 to 5:1 by changing the vanadium resources and imidazole derivatives. Notably, the coordination environment of Ag^+ cations and the structure of POVs in the APFs are also different. Specifically, for **APF-1**, the four Ag atoms adopt three-coordinated and four-coordinated geometries, respectively, and Ag-imidazole complexes and $[V_4O_{12}]^{4-}$ cluster form the one-dimensional polymeric chains. While Ag atoms in **APF-2** and **APF-3** exhibit two-, four- and five-coordinated geometries for **APF-2**, four-, five- and six-coordinated geometries for **APF-3**, respectively. These Ag^+ cations and decavanadate clusters are assembled into the 2D supramolecular structure through the Ag-O bonds and Ag···Ag argentophilic interaction. Remarkably, thus-obtained **APF-2** can serve as powerful efficient heterogeneous catalyst for construction of C–N bond and detoxification of simulant sulfur mustard (yields up to 99%), which enable successful recycling for three cycles with remained catalytic activities and structure stability.

The C–N bond formation as well as the construction of C–C bond is an important chemical transformation in organic syntheses [1–6]. Among these effective approaches of formation of C–N bonds, three-component Mannich reaction is one of the most feasible strategies for preparation of β-amino carbonyl derivatives with C–N bond and it has attracted a considerable amount of attention by synthetic chemists owing to its high atom economy and efficiency over the past few decades [7–10]. In theory, the Mannich coupling process of arylacetylenes and amines is considered to involve the activation of the terminal C–H bond of acetylene by a nucleophile and active metal (Ag, Cu, *etc.*) insertion, therefore the metal catalysts are expected to play a key role in reducing the activation energy of the Mannich reaction, thereby enhancing the catalytic efficiency [11,12]. Thus, there is a rapidly growing topic for the synthesis of functionalized transition-metal catalysts to promote the Mannich reaction in organic conversion. Although the development of a multitude of well-designed catalysts toward Mannich reaction has been presented in the past decade, and the current disadvantages of this process are a certain amount of energy consumed and the reused of catalysts, *etc.* [13]. Therefore, the search for highly active and operated more easily catalyst systems remains one of the longstanding research subjects.

In additionally, 2-chloroethylethylsulfide (CEES), as a dangerous simulant sulfur mustard, is one typical example of a Chemical Weapons Agents (CWAs) that can be a persistent threat to mankind because of its vesicant properties [14,15]. Therefore, it is urgent to develop efficient catalytic materials to detoxicate this dangerous

* Corresponding authors.
E-mail addresses: hxqqxh2008@163.com (X. Huang), lijk0212@163.com (J. Li), erick@ecut.edu.cn (G. Yang).

https://doi.org/10.1016/j.cclet.2021.09.042
1001-8417/

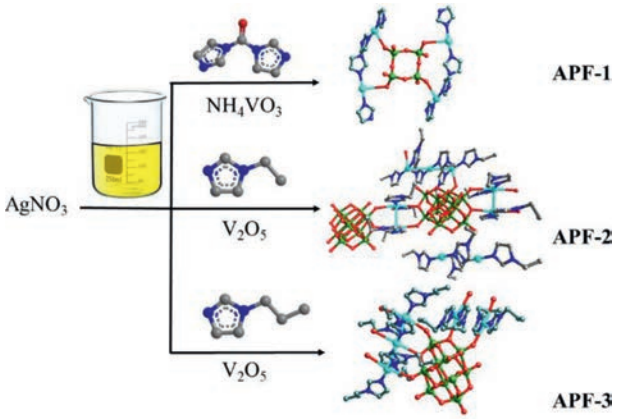

Fig. 1. Simplified ball-and-stick representation of the syntheses of **APFs 1–3**. Color code: Ag, turquiose; V, green; N, blue; O, red; C, gray.

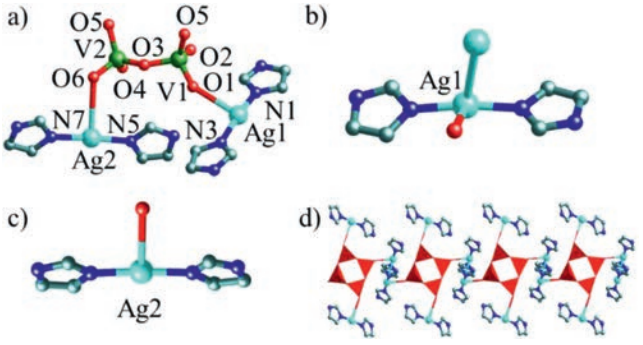

Fig. 2. Simplified ball-and-stick and polyhedron representation of **APF-1**. (a) The asymmetric unit of **APF-1**. (b) The coordination environment of Ag1 atom. (c) The coordination environment of Ag2 atom. (d) The 1D chain structure of **APF-1**. Color code: Ag, turquiose; V polyhedron, red; N, blue; O, red; C, gray.

blistering agent. Thus, the environment friendly outstanding degradation catalytic system at room temperature for CEES is still in exploring [16].

As a representative of multifunctional crystalline materials, polyoxometalates (POMs) is the nanoscale early transition-metal oxide polyanionic clusters and remarkable building blocks in the self- assembly of versatile and intriguing inorganic-organic functionalized hybrids [17–22]. Among POMs materials, the hybrid POVs have been gaining considerable importance and extensive attention in the domain of magnetism, catalysis, energy conversion and fluorescence [23,24], *etc.* Additionally, the transition-metal silver cations, as the soft d^{10} element and the good metal connector, are suitable candidates in the process of synthesizing Ag-decorated hybrids owing to its diverse coordination modes [25–33]. Sun's group first prepared a new silver(I)-based rugby-ball shaped $[Ag_{10}@(W_7O_{26})_2@Ag_{74}]$ with the carboxylate-controlled skeletal isomerism in silver nanoclusters [34]. Recently, Suzuki *et al.* successively synthesized the novel triangular $TBA_9H_4[Ag_7(Si_3W_{27}O_{96})]\cdot 12C_3H_6O$ and atomically precise $TBA_{16}(Me_2NH_2)_8H_5Ag_2[Ag_{27}(Si_6W_{54}O_{198})$ nanocluster and these compounds exhibited the unprecedented ultrastability in both solid and solution states [35,36]. So far, limited research of Ag-complexes modified POVs has developed, for example, Gao and his co-workers reported the self-assembly of metavanadate and silver(I) salts generated a novel dodecahedrane-like $[Ag_{30}(tBuS)_{20}V_{12}O_{34}]\cdot 10CH_3OH$ with the properties of acid-base induced transformation [37]. Xie and Mak isolated two unprecedented neutral silver(I)-ethynide phosphonate-functionized polyoxovanadates giant clusters [38]. Although these elegant works about Ag-POVs have been well demonstrated, their catalytic properties are rarely involved. In this context, the construction of Ag-POVs with a controllable molar ratio of Ag^+ to POVs still remains a challenge [39]. Importantly, the examples of Ag-POVs as catalysts were applied in the field of formation of C–N bond and catalytic degradation for CEES reactions have not been fully explored [40]. Therefore, designing of new Ag-POVs crystalline materials with the efficient catalytic properties in organic conversion is an undoubtedly both highly demanding and challenging task.

Herein, three novel Ag-POVs frameworks, *i.e.*, $[Ag(IM)_2]_2V_4O_{12}\cdot 2Ag(IM)_2$ (**APF-1**), $[Ag_2(1\text{-eIM})_4]_2[Ag(1\text{-eIM})_2]_3\cdot 2Ag(1\text{-eIM})_2[V_{10}O_{28}]_2$ (**APF-2**) and $[Ag(1\text{-pIM})_2]_3[HV_{10}O_{28}]\cdot 2Ag(1\text{-pIM})_2$ (**APF-3**), have been successfully constructed using imidazole derivatives and NH_4VO_3 (or V_2O_5) as initial reaction substrates in water (Fig. 1). Notably, these APFs are further used as effective catalysts in the selective oxidation of CEES and Mannich reaction under mild conditions. Interestingly, **APF-2** presents the excellent heterogeneous catalytic performance (yields up to 99%) superior to its components, **APF-1** and **APF-3**. Furthermore, based on the control experiments and previous results, the two possible mechanisms about the oxidation of CEES and Mannich reaction catalyzed by **APF-2** have been proposed to explain the observed catalytic activities.

As transition-metal hybrid POVs could exhibit the adjustable molecular structures, it is important to develop the reliable synthetic conditions toward some specific transition-metal-POVs structures with a controllable molar ratio of transition metal to POVs [41]. Herein, the reaction between carbonyl diimidazole, 1-ethylimidazole or 1-propylimidazole with NH_4VO_3 or V_2O_5 and $AgNO_3$ in an aqueous solution resulted in the formation of three POVs-based silver hybrids ($[V_4O_{12}]^{4-}$ for **APF-1**, $[V_{10}O_{28}]^{6-}$ for **APF-2** and **APF-3**), respectively. Interestingly, the **APFs 1–3** with diverse coordination modes of Ag^+ cations and different molar ratios of Ag^+ to POVs (from 4:1, 4.5:1 to 5:1) are obtained, which mainly caused by the different base environment and starting materials in the formation of these APFs.

Single-crystal X-ray diffraction measurements reveals that the asymmetric unit of **APF-1** contains two Ag^+ ions, one $[V_2O_6]^{2-}$ anion and four imidazole ligands (derived from carbonyl diimidazole) (Fig. 2a) [42]. The bond valence sum calculations show that both V atoms in the POVs are in $+V$ oxidation state (Table S3 in Supporting information). In **APF-1**, the two crystallographically independent V atoms (V1 and V2) possess the distorted $[VO_4]$ tetrahedron by a terminal O atom and three bridging O atoms, respectively, and further form the $[V_2O_6]^{2-}$ cluster by one of their corner-sharing O3 atom (Fig. 2a). The $[V_2O_6]^{2-}$ cluster is further connected by the other corner-sharing O5 atom to form a $[V_4O_{12}]^{4-}$ cluster. The $[V_4O_{12}]^{4-}$ clusters in **APF-1** act as bridging inorganic ligands and coordinate with four silver centers, as shown in Fig. 2d. Notably, two crystallographically independent Ag1 and Ag2 ions exhibit two types of coordination geometries. The Ag1 center is four-coordinated by one terminal O1 atom from the $[V_4O_{12}]^{4-}$ cluster, two N donors (N1 and N3) from two imidazole ligands and one Ag1#1 ion (#1: -x, 1-y, -z) through the Ag···Ag argentophilic interaction in a distorted trigonal pyramidal geometry (Fig. 2b) [43]. Interestingly, the Ag2 ion is coordinated by one terminal O6 atom from the $[V_4O_{12}]^{4-}$ cluster and two N donors (N5 and N7) from two imidazole ligands, adopting a three-coordinated pattern with a T-type geometry (Fig. 2c). Through the unique Ag···Ag argentophilic interaction, the $[V_4O_{12}]^{4-}$ clusters are further connected together by $[Ag_2(IM)_4]^{2+}$ units to form a 1D chain structure (Fig. 2d).

The molecular structure of **APF-2** consists of two typical $[V_{10}O_{28}]^{6-}$ anions, nine Ag^+ ions and twenty-one 1-eIM ligands (eighteen coordinated 1-eIM and three protonated free 1-HeIM), as shown in Fig. 1. Each $[V_{10}O_{28}]^{6-}$ polyanion of **APF-2** has a crystal-

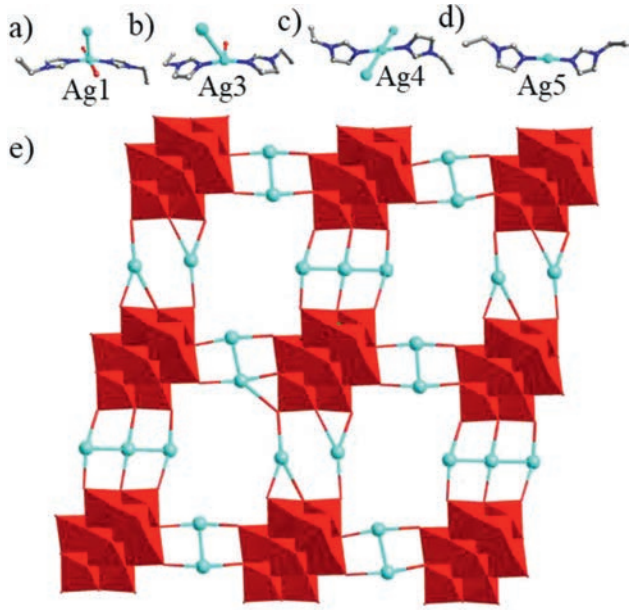

Fig. 3. Simplified ball-and-stick and polyhedron representation of **APF-2**. (a) The coordination environment of Ag1 atom; (b) the coordination environment of Ag3 atom; (c) the coordination environment of Ag4 atom; (d) the coordination environment of Ag5 atom; (e) the 2D network structure of **APF-2**. Color code: Ag, turquiose; V polyhedron, red; N, blue; O, red; C, gray. The 1-eIM ligands are removed for clarity.

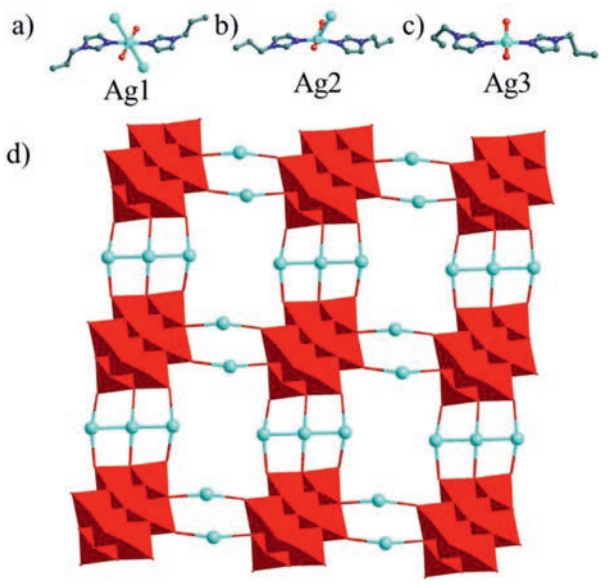

Fig. 4. Simplified ball-and-stick and polyhedron representation of **APF-3**. (a) The coordination environment of Ag1 atom. (b) The coordination environment of Ag2 atom. (c) The coordination environment of Ag3 atom. (d) The 2D network structure of **APF-3**. Color code: Ag, turquiose; V polyhedron, red; N, blue; O, red; C, gray. The 1-pIM ligands are removed for clarity.

lographic center on the midpoint of O19 and O22 and it is made up of ten distorted [VO_6] octahedron, including the highly condensed ten vanadium atoms and twenty-eight different types of oxygen atoms. The bond distances and bond angles of the $[V_{10}O_{28}]^{6-}$ anion are similar with those of reported decavanadate [44,45]. In **APF-2**, these crystallographically independent Ag^+ ions (Ag1 to Ag5) exhibit four types of coordination geometries: (I) The Ag1 and Ag2 ions adopt five-coordinated pattern (Fig. 3a). The Ag1 ion is surrounded by one terminal O1 atom from the $[V_{10}O_{28}]^{6-}$ anion, one bridging O2#1 (#1: 1-x, -y, 1-z) atom from the adjacent $[V_{10}O_{28}]^{6-}$ anion, two N atoms (N1 and N3) from two 1-eIM ligands and one Ag1#1 atom through the Ag…Ag argentophilic interaction, and resulted in a $\{AgN_2O_2\}$ geometry. The Ag2 ion is coordinated by one bridging O25 atom from one $[V_{10}O_{28}]^{6-}$ anion, one terminal O26#2 (#2: 1-x, 1-y, 2-z) atom, two N atoms (N7 and N5#2) from two 1-eIM ligands and one Ag atom (Ag2#2). (II) The Ag3 ion is four-coordinated by two N atoms (N9 and N11) from two 1-eIM ligands, one terminal O atom from one $[V_{10}O_{28}]^{6-}$ anion and the Ag4 atom through the Ag…Ag argentophilic interaction, and the coordination environment of Ag3 employs the $\{AgN_2O\}$ mode (Fig. 3b). (III) The Ag4 ion adopts four-coordinated pattern with square plane geometry (Fig. 3c). The Ag4 ion is surrounded by two N atoms (N13 and N13#3 (#3: 1-x, -y, 2-z) from two 1-eIM ligands and two Ag atoms (Ag3 and Ag3#3), and presents the $\{Ag_2N_2\}$ coordination mode (Fig. 3c). (IV) As depicted in Fig. 3d, Ag5 ion is in linear geometries by two N atoms (N15 and N17) from two 1-eIM ligands. Interestingly, the Ag1 and Ag2 ions connect the adjacent $[V_{10}O_{28}]^{6-}$ anions into a 1D chain structure, and further the adjacent 1D chain structures are connected together to form a 2D network along the *bc* plane (Fig. 3e).

The asymmetric unit of **APF-3** contains five Ag^+ ions, one typical $[HV_{10}O_{28}]^{5-}$ anion and ten 1-pIM ligands (Fig. 1). The $[HV_{10}O_{28}]^{5-}$ anion of **APF-3** has a crystallographic center on the midpoint of O14 and O14#1 (#1: 2-x, -y, 2-z) and it is made up of ten distorted [VO_6] octahedron including the highly condensed ten vanadium atoms and twenty-eight different types of oxygen atoms. In **APF-3**, three crystallographically independent Ag^+ ions (Ag1 to Ag3) exhibit three types of coordination geometries: (I) The Ag1 ion is six-coordinated by two bridging O12 and O12#2 atoms (#2: 1-x, -y, 2-z) from two $[HV_{10}O_{28}]^{5-}$ anions, two N atoms (N1 and N1#2) from two 1-pIM ligands and two Ag atoms (Ag2 and Ag2#), adopting the distorted octahedron geometry (Fig. 4a). (II) The Ag2 ion is five-coordinated by two terminal O11 and O13#2 atoms from two $[HV_{10}O_{28}]^{5-}$ anions, two N atoms (N3#2 and N5#2) from two 1-pIM ligands and one Ag atoms (Ag1) through the Ag···Ag interaction in a $\{AgN_2O_2\}$ mode (Fig. 4b). (III) The Ag3#3 (#3: 2-x, 1-y, 1-z) ion is four-coordinated by one terminal O4 atoms, one bridging O6#3 atoms from two $[HV_{10}O_{28}]^{5-}$ anions and two N atoms (N7#3 and N9#3) from two 1-pIM ligands, displaying the square plane geometry (Fig. 4c). Interestingly, the Ag1 and Ag2 ions connect the adjacent $[HV_{10}O_{28}]^{5-}$ anions into a 1D chain structure along the *a* axis, and further the adjacent 1D chain structures are connected into a 2D network along the *ab* plane (Fig. 4d).

Subsequently, on the basis of determining the structure of APFs, we further investigated the catalytic effectiveness of these APFs in the construction of C–N bond *via* Mannich reaction. In our initial studies, phenylacetylene (**1a**), formaldehyde (**1b**) and piperidine (**1c**) were selected as model substrates to examine the efficiency of these APFs in the construction of C–N bond (Table 1). We conducted the three component reaction under the conditions of **1a** (0.25 mmol), aqueous **1b** (0.5 mmol) and **1c** (0.5 mmol) in CH_3CN (1 mL) in the presence of catalysts at mild conditions for 4 h

To begin, the blank experiment indicated that only trace conversion was achieved in the absence of any catalysts (Table 1, entry 1). The reactants phenylacetylene (**1a)**, formaldehyde (**1b)** and piperidine (**1c)** were smoothly reacted with $AgNO_3$ as the homogeneous catalyst, which gave rise to the desired product 1-(3-phenylprop-2-yn-1-yl)piperidine **1d** in 21% yield (Table 1, entry 3), nevertheless, the scale potential industrial applications of the $AgNO_3$ catalyst have been limited due to its non-reusability. Prompted by this initial observation, the model reaction was thoroughly optimized by varying different parameters, such as catalyst, the amount of catalyst, and reaction time (Table 1). The use of other catalysts like

Table 1
The effect of different parameters on Mannich reaction.[a]

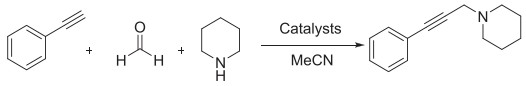

1a 1b 1c 1d

Entry	Catalyst (mol%)	*t* (h)	Yield (%)[b]
1	NA	4	–
2	$Na_6V_{10}O_{28}{\cdot}16H_2O$ (0.5)	4	trace
3	$AgNO_3$ (0.5)	4	21
4	**APF-1** (0.5)	4	72
5	**APF-2** (0.5)	4	83
6	**APF-3** (0.5)	4	77
7	**APF-2** (0.5)	6	86
8	**APF-2** (1.0)	6	92
9	**APF-2** (1.5)	8	99
10	**APF-2** (1.5)	10	99

[a] The reactions were carried out using **1a** (0.25 mmol), **1b** (0.5 mmol), **1c** (0.5 mmol), and catalyst in MeCN (1 mL), 40 °C.
[b] The yields are detected by GC and chlorobenzene was used as internal standard.

APF-1, APF-2 and **APF-3** improved the product yields from 72% to 83%, respectively (Table 1, entries 4–6). **APF-2** with the best performance is selected as the target catalyst for further characterization. Keeping all other parameters of entry 5 as such, the amount of catalyst and reaction time were then examined, which markedly disclosed 1.5 mol% and 8 h as optimum conditions and entry 9 as the best fit. Consequently, the best conditions for synthesis of the 1-(3-phenylprop-2-yn-1-yl)piperidine were optimized as follows: **1a** (0.25 mmol), **1b** (0.5 mmol), **1c** (0.5 mmol) and **APF-2** (1.5 mol%), MeCN (1 mL), 40 °C, 8 h

With the established conditions in hand, the scope and versatility of the reaction were subsequently examined (Table 2). A diverse array of acetylenes containing electron-donating groups such as -Me, -Et, *n*-Pr, *n*-Bu, as well as electron-withdrawing groups such as -Cl, participated nicely with formaldehyde and piperidine under the optimized conditions was amenable to afford the predictable coupling products in excellent yields (up to 99%) (Table 2, entries 1–6). As regards the other amine, gratifyingly, morpholine also worked as the source of amine well to afford the desired Mannich products (Table 2, entries 7–12). More importantly, the excellent catalytic properties of APF-2 in the construction of C–N bonds were comparable with those of the previous results catalysed by POMs catalysts [46]. To investigate the durability and recyclability of the APFs catalysts, the repeated experiments have been conducted in the three-component reaction of phenylacetylene, formaldehyde and morpholine under the optimum conditions in Table 2 and the corresponding results were shown in Fig. 5. After each catalytic cycle, the catalyst was separated from the reaction mixture by centrifugation, washed with ethanol three times and dried at 50 °C for 2 h, and then stored under vacuum. The conversions of phenylacetylene for the three consecutive runs were satisfactory in terms of Mannich product yields (Fig. 5a).

To prove the stability of the catalyst, XPS, PXRD and FT-IR spectra of **APF-2** were recorded, respectively, and the results showed that no significant change was observed in either of them and all the characteristic bands and peaks of these spectra were remaining unaltered before and after the oxidation reaction (Figs. 5b and c, Figs. S7 and S8 in Supporting information). The result strongly suggests that the hybrid **APF-2** is durable and recyclable in the Mannich reaction. Mechanistically, according to the above experiments and previous results, we proposed a plausible mechanism catalyzed by **APF-2** depicted in Fig. 5d [47,48]. First, **APF-2** promoted the formation of intermediate **B** by the interaction of the phenylacetylene and catalyst. Second, species **B** activated the triple

Table 2
Substrate scope for Mannich reaction.[a]

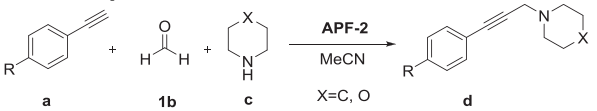

a 1b c d

Entry	R	Products	Conv. (%)	Yield (%)[b]
11	R = H	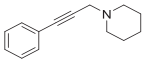	99	99
2	R = Me	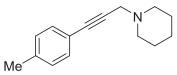	99	98
3	R = Et	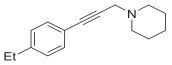	99	99
4	R = *n*-Pr	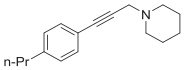	98	98
5	R = *n*-Bu	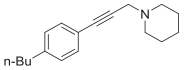	97	97
6	R = Cl	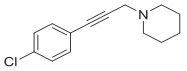	96	95
7	R = H	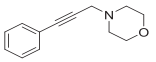	98	97
8	R = Me	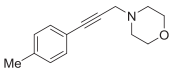	99	99
9	R = Et	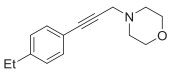	99	99
10	R = *n*-Pr	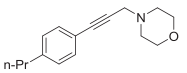	98	98
11	R = *n*-Bu	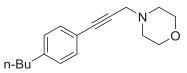	99	98
12	R = Cl	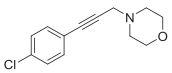	97	97

[a] Reaction conditions: **a** (0.25 mmol), **1b** (0.5 mmol), **c** (0.5 mmol), catalyst (1.5 mol%), MeCN (1 mL), 40 °C, 8 h.
[b] The yields are detected by GC and chlorobenzene was used as internal standard.

bond to form Ag-acetylide intermediate **C** [49,50]. Third, **C** species reacted with the imnium ion originated by the condensation reaction of formaldehyde and piperidine to achieve the desired Mannich product.

In consideration of APFs having the potential to be an oxidation catalyst, the selective oxidation of CEES was investigated under mild conditions, which was considered an effective protocol for detoxification of simulant sulfur mustard. In a typical oxidation of CEES, the reaction conditions are as followed: 0.25 mmol CEES, 5 μmol catalysts, 0.3 mmol H_2O_2, 0.5 mL ethanol at room temperature and the progress of the catalytic reaction was detected by GC, and the product was confirmed by GC–MS. The preliminary optimized results are presented in Fig. 6. As shown in Fig. 6a, a blank experiment without catalyst exhibited less than 20% conversion, nevertheless, when **APFs 1–3** were used as the catalysts, the conversions of CEES reached 76%, 99% and 91%, respectively. These results showed that although **APF-2** has a smaller amount of molar ratio of Ag to polyoxovanadates (4.5:1) than that of **APF-3** (5:1),

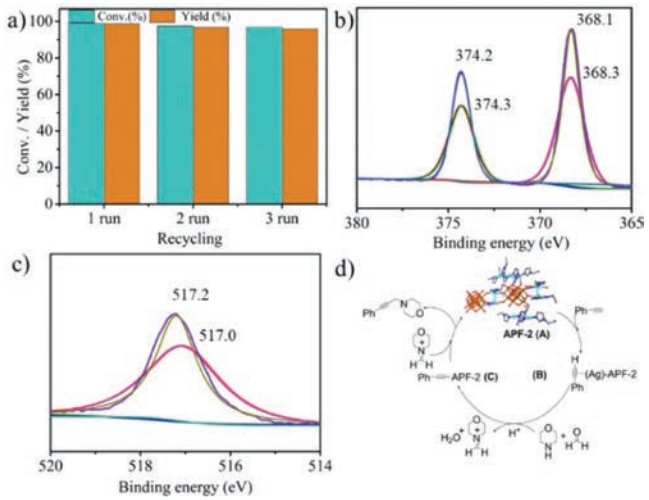

Fig. 5. (a) The results of Mannich reaction catalyzed by **APF-2** in three run experiments. (b) The XPS of Ag in **APF-2** before and after three runs reaction. (c) The XPS of V in **APF-2** before and after three runs reaction. (d) The proposed mechanism for Mannich reaction catalyzed by **APF-2**.

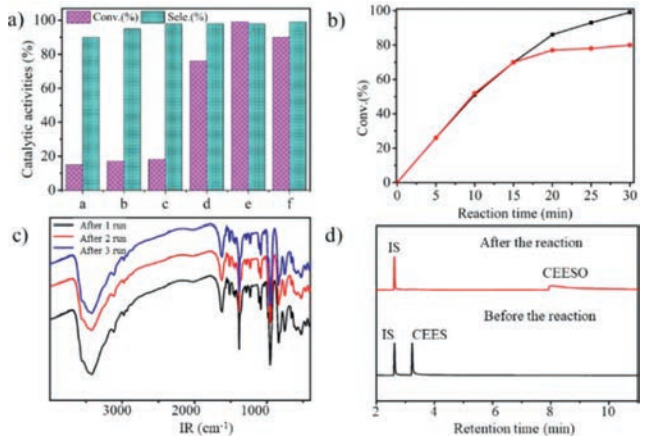

Fig. 6. (a) Reaction conditions: CEES (0.25 mmol), H_2O_2 (0.3 mmol), EtOH (0.5 mL), catalysts (5 μmol), room temperature, 30 min. a: blank; b: $AgNO_3$; c: V_2O_5; d: APF-1; e: **APF-2**; f: **APF-3**. (b) Kinetics of the oxidation of CEES with **APF-2** (black); **APF-2** was filtered from the reaction mixture after 15 min (red). (c) The IR spectra of **APF-2** before and after three runs oxidation of CEES. (d) The GC spectrum of before and after the oxidation of CEES catalyzed by **APF-2**.

the conversion of CEES using **APF-2** as the catalyst was still higher than that of **APF-3**, demonstrating that the coordination environment of Ag^+ and the POVs structures played an important role in their detoxification activity of simulant sulfur mustard.

Consequently, to illuminate the role of each active component of **APF-2** in the oxidative degradation of CEES, a series of control experiments were performed. When using $AgNO_3$ and $TBA_6V_{10}O_{28}$ as catalyst comparisons under similar conditions and the results were exhibited in the Fig. 6a. It was clearly that the highest conversion of 99% could be reached with **APF-2**, while for $AgNO_3$, V_2O_5 after 30 min, the conversions were far below that of **APF-2**, respectively. Overall, we concluded that the high-efficiency catalytic performance of **APF-2** in oxidation of CEES might be resulted by the synergy of Ag^+ sites and decavanadate center after coordination polymerization. These results indicated that almost all of the CEES was removed and **APF-2** could be employed as an effective catalyst in the removal of CEES, compared to the POVs-based inorganic-organic hybrids $[Co(bib)]\{V_2O_6\}$ and $[Ni(bib)_2]\{V_2O_6\}$ (bib = 1,4-bis(1*H*-imidazoly-1-yl)benzene) [51,52].

To evaluate the reusability and stability of **APF-2** for its actual application, the leaching test and three runs reusability of oxidation of CEES were carried out under the optimal conditions. The results exhibited that catalyst was filtered from the reaction solution after 15 min, and the conversion of CEES in the resulting solution was basically maintained under identical conditions for another 15 min (Fig. 6b). Remarkably, in the reusability experiment, the conversion was reduced by only 2% after three runs of catalytic reactions [Conv. of CEES: 99% (first run), 98% (second run), 97% (third run)] (Fig. S9 in Supporting information). Furthermore, the IR proved that the structural integrity of APF-2 after catalysis remained unchanged, indicating that the catalyst was an excellent heterogeneous catalyst for CEES oxidation under mild conditions (Fig. 6c). Additionally, GC were also tested before and after the degradation of CEES in the presence of **APF-2** as catalyst and the results were given in Fig. 6d, which suggested that simulant sulfur mustard was almost completely converted to the corresponding nontoxic CEESO products within 30 min under mild conditions.

According to previous investigations on the oxidation CEES of POMs, the POVs can generate active peroxo-metal species in the presence of H_2O_2, which plays an important role in the oxidative reaction [53,54]. Therefore, we speculated the resulting peroxovanaium species are the active species in the detoxification of CEES over **APF-2**. Based on the above experiment and previous reports, we proposed a possible mechanism of CEES degradation with **APF-2** (Fig. S23 in Supporting information). The vanadium of **APF-2** interacts with H_2O_2 to produce active peroxovanadium species (Fig. S24 in Supporting information) [55,56], which subsequently is attacked by the sulfur atom of CEES, thus achieving the corresponding nontoxic product CEESO.

In summary, three APFs with imidazole-modified Ag-complexes as the cations and POVs as the anion were successfully synthesized and fully characterized. Interestingly, the molar ratios of Ag to POVs in the three compounds are controlled by using different imidazole N-containing ligands. More importantly, **APF-2** exhibits excellent bifunctional catalytic performance in the construction C–N bonds and oxidative detoxification of CEES under mild conditions. The high efficiencies validated APFs not only expands the structure of the POVs but also provides insight into the design of bifunctional catalysts with synergistic catalytic properties for organic reactions. Investigations on using these APFs catalysts for other catalytic reactions are in progress.

Declaration of competing interest

The authors report no declarations of interest.

Acknowledgments

The work was financially supported by the National Natural Science Foundation of China (Nos. 21871125, 21871026 and 22001034); the Natural Science Foundation of Shandong Province, China (Nos. ZR2019MB043 and ZR2019QB022), and the Construction Project of Quality Curriculum for Postgraduate Education of Shandong Province (No. SDYKC19057).

Supplementary materials

Supplementary material associated with this article can be found, in the online version, at doi:10.1016/j.cclet.2021.09.042.

References

[1] Q. Wang, Y. Su, L. Li, et al., Chem. Soc. Rev. 45 (2016) 1257–1272.
[2] J.M. Ganley, P.R.D. Murray, R.R. Knowles, ACS Catal. 10 (2020) 11712–11738.
[3] G. Yang, Y. Liu, X. Lin, et al., Chin. Chem. Lett. 33 (2022) 354–357.
[4] G. Yang, Y. Liu, K. Li, et al., Chin. Chem. Lett. 31 (2020) 3233–3236.

[5] J.A. Walker, K.L. Vickerman, J.N. Humke, et al., J. Am. Chem. Soc. 139 (2017) 10228–10231.
[6] W. Yao, Y. Zhang, H. Zhu, C. Ge, D. Wang, Chin. Chem. Lett. 31 (2020) 701–705.
[7] W. Wen, M.J. Luo, Y. Yuan, et al., Nat. Commun. 11 (2020) 5372.
[8] B.M. Trost, J.S. Tracy, T. Yusoontorn, et al., Angew. Chem. Int. Ed. 59 (2020) 2370–2374.
[9] H.J. Zhang, Y.C. Xie, L. Yin, Nat. Commun. 10 (2019) 1699.
[10] J.J. Tian, N. Liu, Q.F. Liu, et al., J. Am. Chem. Soc. 143 (2021) 3054–3059.
[11] C.C. Meyer, E. Ortiz, M.J. Krische, Chem. Rev. 120 (2020) 3721–3748.
[12] N.F. Curtis, Coord. Chem. Rev. 366 (2018) 109–134.
[13] X.Y. Zhang, P.H. Dou, W.Y. Lu, et al., Chem. Commun. 57 (2021) 2927–2930.
[14] R. Gil-San-Millan, E. López-Maya, M. Hall, et al., ACS Appl. Mater. Interfaces 9 (2017) 23967–23973.
[15] M. Florent, D.A. Giannakoudakis, T.J. Bandosz, Appl. Catal. B: Environ. 272 (2020) 119038.
[16] S.G. Xia, Z. Zhang, J.N. Wu, et al., Appl. Catal. B 284 (2021) 119703.
[17] L. Qiao, M. Song, A. Geng, et al., Chin. Chem. Lett. 30 (2019) 1273–1276.
[18] M. Zhao, X.Y. Zhu, Y.Z. Li, et al., Tungsten 4 (2022) 121–129.
[19] P. Mialane, C. Mellot-Draznieks, P. Gairola, et al., Chem. Soc. Rev. 50 (2021) 6152–6220.
[20] B.E. Petel, R.L. Meyer, M.L. Maiola, et al., J. Am. Chem. Soc. 142 (2020) 1049–1056.
[21] H. Bian, X. Zhang, H. Zhao, et al., Chin. Chem. Lett. 30 (2019) 1097–1099.
[22] G.P. Yang, X.L. Zhang, Y.F. Liu, et al., Inorg. Chem. Front. 8 (2021) 4650–4656.
[23] H.R. Tian, Y.W. Liu, Z. Zhang, et al., Green Chem. 22 (2020) 248–255.
[24] J.P. Cao, Y.S. Xue, N.F. Li, et al., J. Am. Chem. Soc. 141 (2019) 19487–19497.
[25] Z. Xu, K. Chen, M. Li, et al., Chem. Commun. 56 (2020) 5287–5290.
[26] W.J. Zhang, Z. Liu, K.P. Song, et al., Angew. Chem. Int. Ed. 60 (2021) 4231–4237.
[27] Z. Wang, M. Ashafaq, Y.F. Lu, et al., Inorg. Chem. 60 (2021) 2899–2904.
[28] Z. Wang, L.M. Zheng, M. Jagodič, et al., Inorg. Chem. 59 (2020) 3004–3011.
[29] Y. Hou, H. Pang, C.J. Gómez-García, et al., Inorg. Chem. 58 (2019) 16028–16039.
[30] C. Deng, C. Sun, Z. Wang, et al., Angew. Chem. Int. Ed. 59 (2020) 12659–12663.
[31] Z. Wang, J.W. Liu, H.F. Su, et al., J. Am. Chem. Soc. 141 (2019) 17884–17890.
[32] J.W. Liu, L. Feng, H.F. Su, et al., J. Am. Chem. Soc. 140 (2018) 1600–1603.
[33] M. Zhao, S. Huang, Q. Fu, et al., Angew. Chem. Int. Ed. 59 (2020) 20031–20036.
[34] Z. Wang, H.T. Sun, M. Kurmoo, et al., Chem. Sci. 10 (2019) 4862–4867.
[35] K. Yonesato, H. Ito, D. Yokogawa, et al., Angew. Chem. Int. Ed. 59 (2020) 16361–16365.
[36] K. Yonesato, S. Yamazoe, D. Yokogawa, et al., Angew. Chem. Int. Ed. 60 (2021) 16994–16998.
[37] H. Liu, C.Y. Song, R.W. Huang, et al., Angew. Chem. Int. Ed. 55 (2016) 3699–3703.
[38] Y.P. Xie, T.C.W. Mak, J. Am. Chem. Soc. 133 (2011) 3760–3763.
[39] A.A. Shmakova, A.S. Berezin, P.A. Abramov, et al., Inorg. Chem. 59 (2020) 1853–1862.
[40] X.X. Li, L.J. Zhang, C.Y. Cui, et al., Inorg. Chem. 57 (2018) 10323–10330.
[41] X. Huang, J. Li, G. Shen, et al., Dalton Trans. 47 (2018) 726–733.
[42] T.C. Stamatatos, S.P. Perlepes, C.P. Raptopoulou, et al., Dalton Trans. 17 (2009) 3354–3362.
[43] C. Sun, B.K. Teo, C. Deng, et al., Coord. Chem. Rev. 427 (2021) 213576.
[44] X. Huang, X. Gu, H. Zhang, et al., J. CO_2 Util. 45 (2021) 101419.
[45] H. An, J. Zhang, S. Chang, et al., Inorg. Chem. 59 (2020) 10578–10590.
[46] X. Huang, X. Gu, Y. Qi, et al., Chin. J. Chem. 39 (2021) 2495–2503.
[47] L.P. Zorba, G.C. Vougioukalakis, Coord. Chem. Rev. 429 (2021) 213603.
[48] O. Prakash, H. Joshi, U. Kumar, et al., Dalton Trans. 44 (2015) 1962–1968.
[49] M.T. Chen, B. Landers, O. Navarro, Org. Biomol. Chem. 10 (2012) 2206–2208.
[50] P. Li, M. Wang, Y. Zhang, et al., Tetrahedron Lett. 49 (2008) 6650–6654.
[51] H.R. Tian, Z. Zhang, S.M. Liu, et al., J. Mater. Chem. A 8 (2020) 12398–12405.
[52] H.R. Tian, Z. Zhang, T.Y. Dang, et al., Inorg. Chem. 60 (2021) 840–845.
[53] N. Zhen, J. Dong, Z. Lin, et al., Chem. Commun. 56 (2020) 13967–13970.
[54] J. Dong, J. Hu, Y. Chi, et al., Angew. Chem. Int. Ed. 56 (2017) 4473–4477.
[55] Y. Hou, H. An, S. Chang, et al., Catal. Sci. Technol. 9 (2019) 2445–2455.
[56] Y.J. Hou, H.Y. An, Y.M. Zhang, et al., ACS Catal. 8 (2018) 6062–6069.